



ELSEVIER

Contents lists available at SciVerse ScienceDirect

Journal of Luminescence

journal homepage: www.elsevier.com/locate/jlumin

Rate equation modelling of erbium luminescence dynamics in erbium-doped silicon-rich-silicon-oxide

Miraj Shah^{a,*}, Maciej Wojdak^a, Anthony J. Kenyon^a, Matthew P. Halsall^b, Hang Li^b, Iain F. Crowe^b

^a Department of Electronic & Electrical Engineering, UCL, Torrington Place, London WC1E 7JE, United Kingdom

^b Photon Science Institute and School of Electrical & Electronic Engineering, University of Manchester, Sackville St Building, Manchester M13 9PL, United Kingdom

ARTICLE INFO

Available online 1 March 2012

Keywords:

Erbium cluster
Si-nanocrystal
Rate equations
Lifetimes
Ion–ion interactions
Energy migration

ABSTRACT

Erbium doped silicon-rich silica offers broad band and very efficient excitation of erbium photoluminescence (PL) due to a sensitization effect attributed to silicon nanocrystals (Si-nc), which grow during thermal treatment. PL decay lifetime measurements of sensitised Er³⁺ ions are usually reported to be stretched or multi exponential, very different to those that are directly excited, which usually show a single exponential decay component.

In this paper, we report on SiO₂ thin films doped with Si-nc's and erbium. Time resolved PL measurements reveal two distinct 1.54 μm Er decay components; a fast microsecond component, and a relatively long lifetime component (10 ms). We also study the structural properties of these samples through TEM measurements, and reveal the formation of Er clusters. We propose that these Er clusters are responsible for the fast μs decay component, and we develop rate equation models that reproduce the experimental transient observations, and can explain some of the reported transient behaviour in previously published literature.

© 2012 Elsevier B.V. All rights reserved.

1. Introduction

Over the past decade, erbium doped Si-nanocrystals (Si-nc) have attracted a great deal of attention, due to the enhanced emission from erbium sensitised through Si-nc's [1]. The 1.54 μm emission line of erbium is ideal for telecommunication purposes as it lies within the minimum propagation loss for silica fibres. Also, the broad absorption band of Si-ncs allows broadband excitation of erbium, enabling the realisation of an efficient broadband top pumped EDWA. Yet, to date, achieving gain from this material has proven to be a notoriously difficult task. This is, in part, due to the low excitable Er fraction sensitised through Si-ncs. Processes such as excited state absorption, Auger back-transfer, or defect-induced non-radiative paths have all been offered as possible explanations for this low fraction.

Given that there are claims of an enhanced excitation rate, [2,3] and of a distance dependence on excitation of Er ions through Si-ncs, [4] another set of processes that deserve attention are ion–ion interactions. Up-conversion between two Er ions is a well-known effect in existing Er doped amplifiers, and its effect is likely to increase with higher excitation rates. Forms of up-conversion include (i) Pair-induced quenching [5], resulting in the loss of 1 out of every 2 excited

Er ions, and (ii) Energy migration, which extends the overall sensitization distance of Er ions [6].

Er decay lifetime measurements are indicative of such processes. Up-conversion effects usually result in a stretched, or multi, exponential decay component. In fact, for the Er doped Si-nc material, there have been many reports of a fast μs fast-decay component, in addition to the usual slow ms scaled decay. The origin of the fast decay component is still under debate through different interpretations: energy back-transfer to carriers confined in Si-nc [7], deep trap centres [8], recombination at defect centres in SiO₂ or SiO₂/Si-nc interfaces [9].

Recent reports on this material have also shown evidence that the Er ions are not uniformly distributed in the matrix; instead, they agglomerate and form clusters [10]. Even though erbium aggregation has been reported to cause quenching, in some cases, enhanced emission has been reported from these clusters [11].

In this work, the luminescence decay dynamics of Er doped Si-nc samples containing Er clusters are measured experimentally and modelled through rate equations. Strong ion–ion interactions that can be expected to occur in Er clusters result in a microsecond decay component, similar to that observed for our samples and amongst various other groups. We propose that the fast and slow components are a result of ion–ion interactions between Er ions in Er clusters. The cluster size dependence, the clustered fraction of the material, and the fraction of the cluster that is sensitised by the Si-nc will be studied through rate equation

* Corresponding author. Tel.: +44 20 7679 2162/32162.
E-mail address: m.shah@ee.ucl.ac.uk (M. Shah).

analysis, and the results discussed. We find that the random nature of the fast component (in terms of amplitude and rate) can be explained through the interactions in Er rich clusters.

2. Experimental

SiO_x:Er thin films were grown by PECVD on <1 0 0> silicon wafers, using N₂O, 5% SiH₄ diluted in N₂, and Er(thd)₃ precursor evaporated in a bubbler and carried by Ar gas as precursors. Three samples were grown by PECVD with different flow rates of silane, in order to obtain different levels of Si excess. The flow rates of diluted silane (5% of SiH₄ in N₂) were 30, 50, and 80 sccm for samples S1, S2, and S3, respectively. The other deposition conditions were kept the same: flow rate of N₂O (10 sccm), flow rate of Er(thd)₃:Ar (50 sccm), substrate temperature (300 °C) and deposition time (3 h). Subsequently, the samples were annealed at 1100 °C for 1.5 h in flowing Ar gas.

PL measurements were performed using a Bentham M300 single grating monochromator and a NIR-sensitive Hamamatsu photomultiplier (R5509-72). Time-resolved PL transients were recorded with a digital oscilloscope, and the laser was modulated with a Pockels cell. For indirect excitation of erbium luminescence a DPSS laser emitting at a wavelength of 473 nm was used. Direct excitation of erbium was obtained with a Spectra Diode Laboratories MOPA laser emitting at a wavelength of 980 nm.

Conventional bright field (BF) TEM imaging was carried out on Tecnai FEG-30 operating at 300 keV. The chemical composition of the three samples has also been obtained. An aberration corrected STEM, at the Super STEM Laboratory Daresbury, fitted with a Nion Mark II quadrupole–octupole corrector operating at 100 keV was employed to acquire high resolution phase contrast (HRTEM), bright field (BF) and high angle annular dark field (HAADF). The instrument allows Z-contrast lattice images with 1 Å resolution to be obtained.

3. Experimental results

All three samples show strong erbium PL under direct excitation (980 nm). With indirect excitation (473 nm) very weak PL is observed, which increases with Si excess. The PL spectra obtained with both excitation methods are shown in Fig. 1. Note that, for indirect excitation, wider monochromator slits were used during the measurements because of the very weak PL intensity.

Decay transient data is shown in Fig. 2. Direct excitation of erbium leads to nearly single exponential decay characteristics with a long time constant of about 14 ms. This relatively long lifetime indicates a high quality matrix. For indirect excitation, the best fits are double exponential functions of the form $A \exp(-t/\tau_1) + B \exp(-t/\tau_2)$, with long components having time constants close to those observed with direct excitation (10 ms). This is among the longest lifetimes reported for similar materials. A fast component of the order of μ s is also observable. A summary of the transient fits for both direct and in-direct excitation is shown in Table 1. No apparent correlation can be made for the random nature of the microsecond component. It is most prominent in S3 and S1, but hardly observable in S2.

Fig. 3 shows TEM images for samples S1, S2, and S3. We see evidence of Si-ncs in S2 and S3 ranging from a size of 2–5 nm, but none in S1, probably due to low Si excess contents, or the detection limit of the apparatus. Along with Si-ncs, erbium-rich agglomerates, or clusters, are also shown. The chemical compositions of these Er clusters have been studied through electron energy loss spectroscopy (EELS). At the high energy loss region, the EELS spectra reveal that a pre-peak before the main SiO₂ O–K

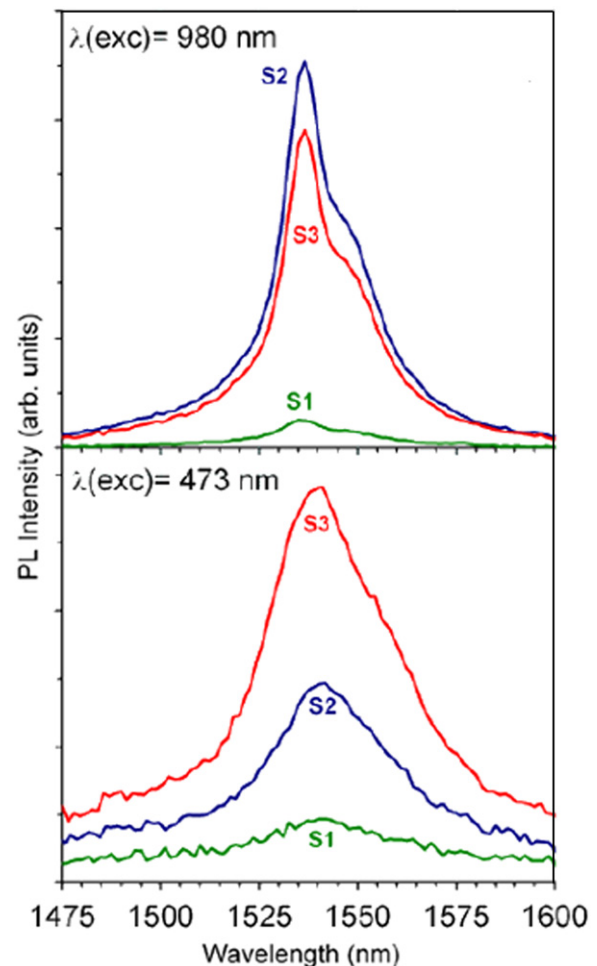


Fig. 1. Erbium PL spectra for both direct (top) and in-direct (bottom) excitation.

edge peak appears in the Er cluster region, and indicates that these Er clusters are oxidised in SRSO film and likely to be Er₂O₃.

The size distribution of these clusters has also been obtained through HAADF measurements. Fig. 4 shows the size distribution for the erbium clusters for samples S1, S2, and S3. We see rather large clusters, particularly in S2 ($\approx 17 \text{ nm}$). In fact, if we look closer at the size distribution and the amplitude and rate of the fast component in Table 1, we see that a direct correlation can be made. For large clusters, the amplitude of the fast component is small and its rate is very fast. So, perhaps these clusters are responsible for the observed decay dynamics.

4. Theory/Modelling

We attempt to explain the observed transient results through rate equation modelling. Rate equations for erbium clusters in glass have been extensively studied [12] and show both fast and slow components. The fast component is a result of strong ion–ion interactions that can be expected to occur for erbium ions in Er-rich clusters. In this work, the fast component only becomes significant and observable for high pumping rates. Due to the 3–4 orders of magnitude increase in the effective excitation cross section through Si-ncs, we know that the pumping rate of erbium ions is also increased by a similar factor. This, together with the evidence of erbium clusters, suggests that the microsecond decay components are due to ion–ion interactions between erbium ions closely spaced in erbium rich clusters.

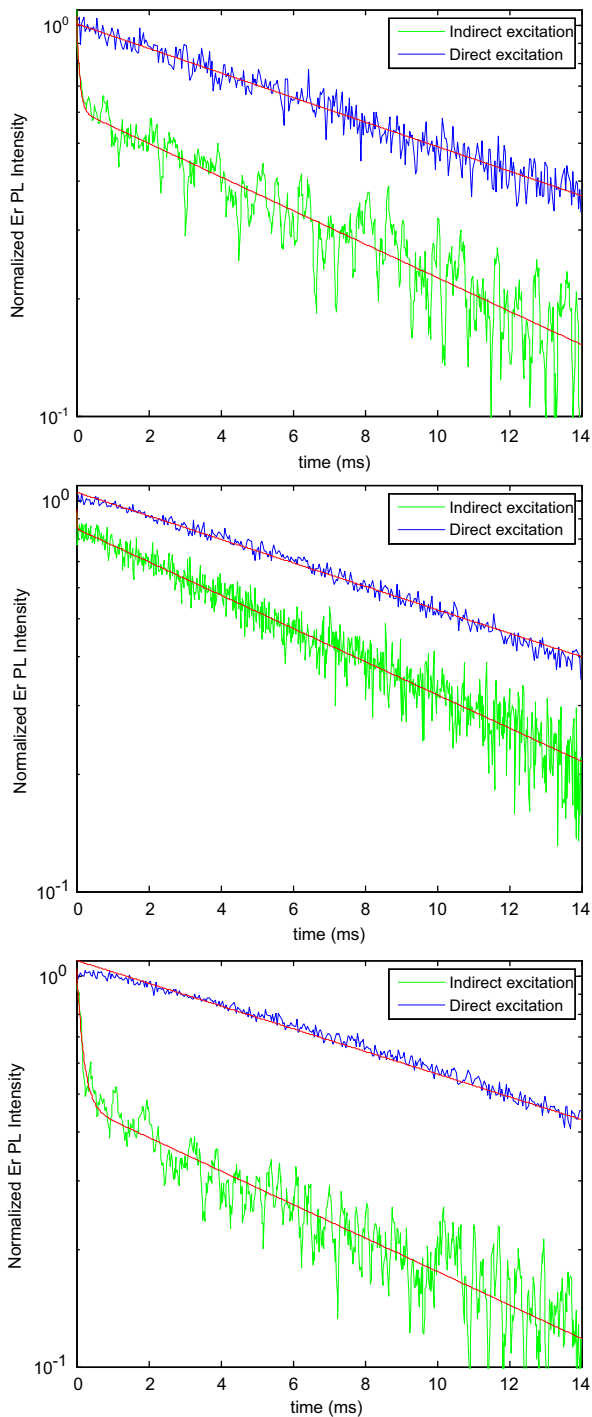


Fig. 2. Erbium PL decay transients for samples S1 (top), S2 (middle) and S3 (bottom), under both indirect and direct excitation.

We assume that only one ion in the cluster is sensitised by the Si-nc (more on this assumption later). Excitation then migrates within the cluster through a cross-relaxation interaction between erbium ions. This is depicted in Fig. 5.

Two specific ion–ion interactions are modelled in this work. The first one, shown in Fig. 6(a) describes the interaction between an excited ion and a ground state ion, where energy is “swapped” between 2 ions, leaving an excited ion in the ground state, and a ground state ion in an excited state. This process is known as energy migration. The second process, shown in Fig. 6(b) describes the pair-induced quenching phenomena. This interaction involves the

Table 1

A summary of the fitting parameters for the erbium PL decay transients under both in-direct and direct excitation. Indirect excitation fits are of the form $A \exp(-t/\tau_1) + B \exp(-t/\tau_2)$, direct excitation fits are of the form $A \exp(-t/\tau_1)$.

	S1	S2	S3
In-direct excitation			
A	0.44	0.10	0.56
B	0.61	0.85	0.47
τ_1 (μ s)	79.49	4.47	161.03
τ_2 (ms)	10.12	10.21	10.11
Direct excitation			
A	1.01	1.06	1.10
τ_1 (ms)	13.79	14.43	14.71

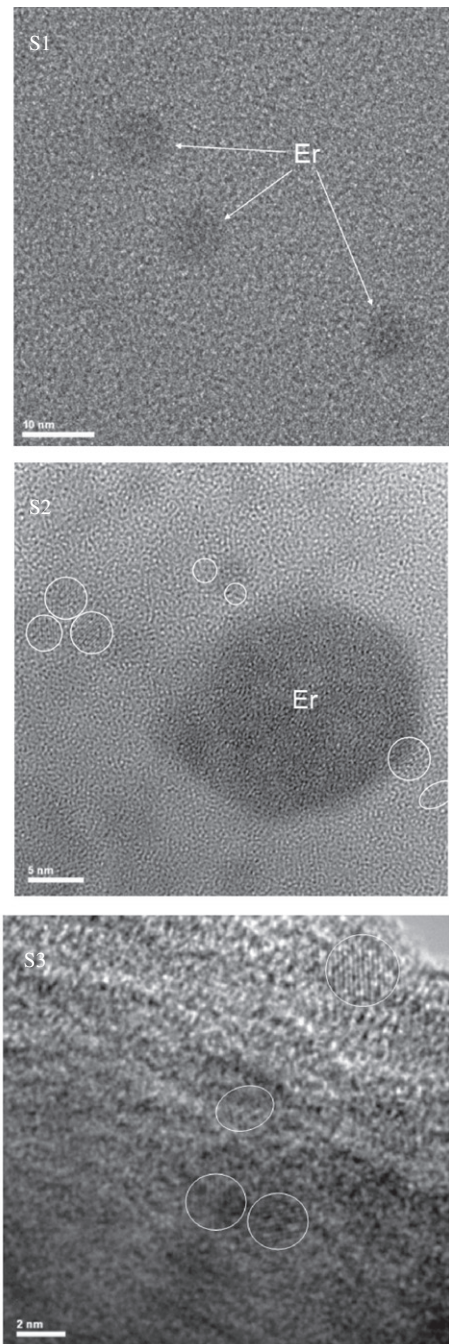


Fig. 3. TEM of samples S1, S2, and S3. Dark areas are erbium agglomerates. Areas in white circles are Si-ncs.

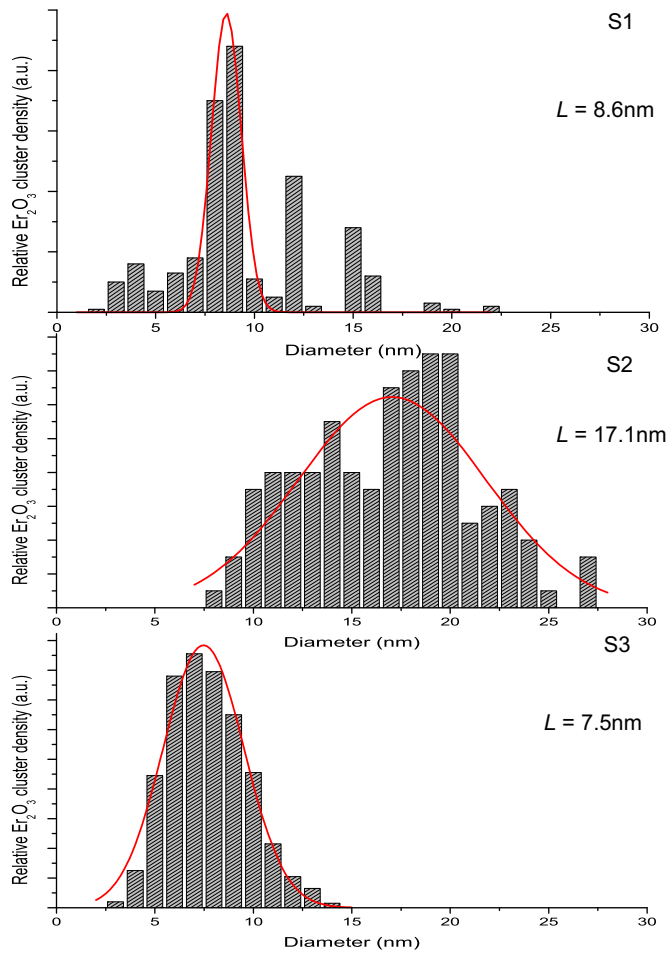


Fig. 4. Erbium cluster size distribution for samples S1, S2, and S3. L is the average cluster diameter.

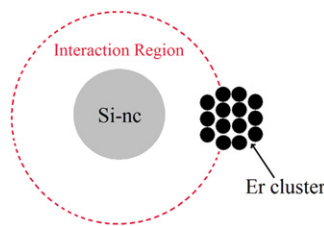


Fig. 5. Schematic illustration of Si-nc coupled to an erbium cluster. Only the ions that fall within the Si-nc interaction region will be available for excitation. The rest of the ions will be excited through energy migration.

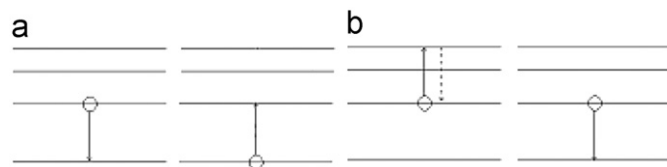


Fig. 6. Illustration of (a) energy migration and (b) pair-induced quenching.

coupling of two excited state erbium ions, whereby one ion gives up its energy by promoting the other ion to an even higher excited state, followed by fast non-radiative relaxation to the initial excited state. The end result of this process is a loss of 1 out of every 2 excited ions, which will limit the total excited proportion of erbium ions, and degrade amplifier performance.

In-direct excitation of erbium ions is mediated through a Si-nc. We model the Si-nc as a 2-level system, in the same fashion adopted by Pacifici et al. [13]. Here, the concentration of excitons, is represented by n_b , and the ground state population is represented by n_a . The excitation cross section of the Si-nc is σ_{ab} , which represents the creation of an exciton following the absorption of a 473 nm photon. w_b is the total decay transition rate for the Si-nc, including both radiative and non-radiative transitions. Excitation of erbium ions through the Si-nc is described by the coupling coefficient A , which describes the interaction between an exciton and a ground state erbium ion. The radiative rate of erbium ions is given as w_{rad} , and we assume that this value is unaffected by erbium clusters.

In order to model the interaction between erbium ions, we set up rate equations describing the population of a group of erbium ions. Initially, the erbium cluster is modelled as an ion-pair, where only one ion in the pair is coupled to the Si-nc. Each ion in the pair is modelled as a 2-level system. Therefore, an ion-pair can be in either 1 of 4 states; a ground state ($N1$) where both ions in the pair are in a ground state, a singly excited state ($N2, N3$) where either the first or second ions in the pair are excited, and a doubly excited state ($N4$), where both ions in the pair are excited. A schematic of the model and all possible pair states are shown in Fig. 7.

So, the Si-nc will essentially “pump” the pair from state ($N1$) to state ($N2$). The singly excited pair can then transfer its energy to the 2nd erbium ion via cross relaxation, moving the pair from state ($N2$) to state ($N3$). The first erbium ion in state ($N3$) can then be re-excited via the Si-nc, bringing the pair into state ($N4$). Note that we can never go directly from state ($N1$) to state ($N4$) via 473 nm (in-direct) pumping, we must go through state ($N2$) and then state ($N3$), due to the distance-dependent interaction with the Si-nc.

Radiative relaxation (emission of a 1.54 μm photon) will also bring the pair into a different state. For example, radiative relaxation of state ($N2$) or state ($N3$) will bring the pair back to the ground state ($N1$).

The pair-induced quenching process involves the interaction between two excited erbium ions, so it will affect the population of $N4$. One ion in the pair will drop to the ground state, while the

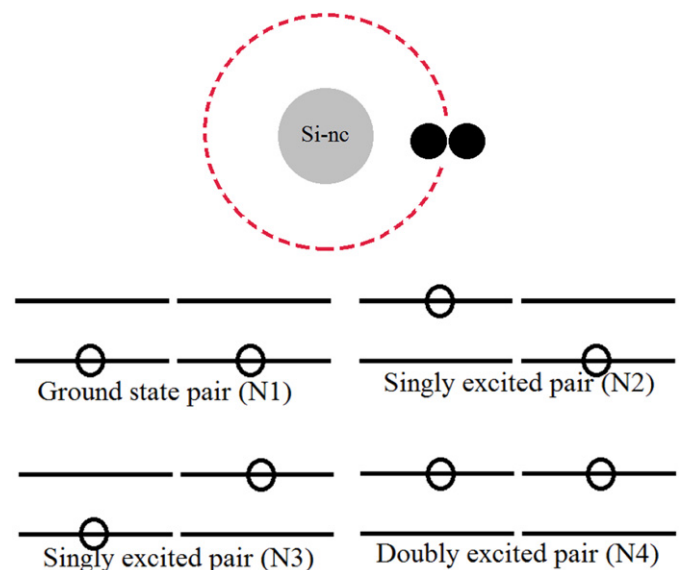


Fig. 7. Diagram of ion-pair model (top) and schematic of all ion pair states (bottom); ground state pair ($N1$), singly excited pairs ($N2, N3$) and doubly excited pair ($N4$).

other ion is excited to higher levels, followed by fast non-radiative decay back down to the initial excited state. This will bring a state (N_4) pair into either state (N_2) or state (N_3).

Under direct pumping, say with a 980 nm laser, the distance dependence is no longer an excitation limit, and all ions in the cluster can be excited. So, in this case, any individual ion in a pair can be excited.

Thanks to this scheme, we are able to write a set of rate equations describing the interactions between a Si-nc and an erbium ion pair, along with the interactions within the erbium ion pair:

$$\frac{dn_a}{dt} = -\sigma_{ab}\varphi_1 n_a + w_b n_b + An_b N_1 + An_b N_3$$

$$\frac{dn_b}{dt} = \sigma_{ab}\varphi_1 n_a - w_b n_b - An_b N_1 - An_b N_3$$

$$\frac{dN_1}{dt} = -An_b N_1 + w_{rad}(N_2 + N_3) - 2BN_1\varphi_2 \quad (1a)$$

$$\frac{dN_2}{dt} = An_b N_1 + w_{Er}(N_3 - N_2) + w_{rad}(N_4 - N_2) + w_p N_4 + B\varphi_2(N_1 - N_2)$$

$$\frac{dN_3}{dt} = -An_b N_3 + w_{Er}(N_2 - N_3) + w_{rad}(N_4 - N_3) + w_p N_4 + B\varphi_2(N_1 - N_3)$$

$$\frac{dN_4}{dt} = An_b N_3 - 2w_{rad}N_4 - 2w_p N_4 + B\varphi_2(N_2 - N_3) \quad (1b)$$

The first set of Eq. (1a) represents creation of an exciton in the Si-nc, followed by either radiative de-excitation, or transfer to clustered erbium ions. The second set of Eq. (1b) represents the behaviour of erbium ion pairs, described earlier. 'B' represents the direct absorption co-efficient of erbium ions for resonant pumping, and φ_1 and φ_2 are the pump fluxes for both in-direct and direct excitation, respectively. w_p and w_{Er} are the energy migration and pair induced quenching rates, described earlier. It is assumed that back-transfer of energy from an excited Er ion to a Si-nc does not occur, due to the energy mismatch between the Si-nc band and the $^4I_{13/2} - ^4I_{15/2}$ band, and due to the relatively small co-efficient for this interaction reported in previous literature [13,14].

The time evolution of each population can be obtained through the solutions of these rate equations. The decay dynamics of the populations are obtained by setting the pump flux to 0, and solving the equations with the saturated levels of each population as inputs. We are interested in the decay dynamics of the 1.54 μm signal, since it relates to the observed experimental transient measurements. The total population of excited state erbium ions ($N_{1.54 \mu\text{m}}$) will be given as $N_{1.54 \mu\text{m}} = N_2 + N_3 + 2N_4$. A summary of the physical parameters used in the rate equation simulations is given in Table 2.

Note that, the number of Er ions within any given cluster presented in Fig. 3 is much greater than that considered in our ion-pair model. Nevertheless, the model still describes the processes that are likely to occur in an Er cluster. And, with further modelling of this nature, we can examine any correlation between cluster size and decay dynamics. In order to assess the effects of cluster size, the modelled cluster is then extended from an ion pair to an ion triplet and ion quadruplet, assuming the same interactions as with the ion pair model. These schematics are shown in Fig. 8. Again, it is assumed that only one ion in the cluster is coupled to the Si-nc, and there are ion-ion interactions between erbium ions within the cluster. The equations for these cluster geometries are shown in Appendix A and B.

Table 2
Parameter values and initial concentrations used in Eq. (1).

Parameter values		Reference
A	$3 \times 10^{-15} \text{ cm}^3 \text{ s}^{-1}$	[13]
B	$1 \times 10^{-19} \text{ cm}^3 \text{ s}^{-1}$	[13]
σ_a	$2 \times 10^{-16} \text{ cm}^2$	[13]
φ_1	$8.5 \times 10^{19} / \text{cm}^{-2} \text{ s}^{-1a}$	
φ_2	$1.75 \times 10^{20} / \text{cm}^{-2} \text{ s}^{-1b}$	
w_b	$2 \times 10^4 \text{ s}^{-1}$	[13]
w_{rad}	100 s^{-1}	
w_{Er}	10000 s^{-1}	[12]
w_p	10000 s^{-1}	[12]
Initial concentrations		
N1	$2.5 \times 10^{19} \text{ cm}^{-3c}$	
N2, N3, N4	0	
n_b	0	
n_a	$1 \times 10^{19} \text{ cm}^{-3}$	

^a For 473 nm excitation wavelength, 100 mW pump power.

^b For 980 nm excitation wavelength, 100 mW pump power.

^c N1 is ion pairs, so total number of ions = $2N_1 = 5 \times 10^{19}$.

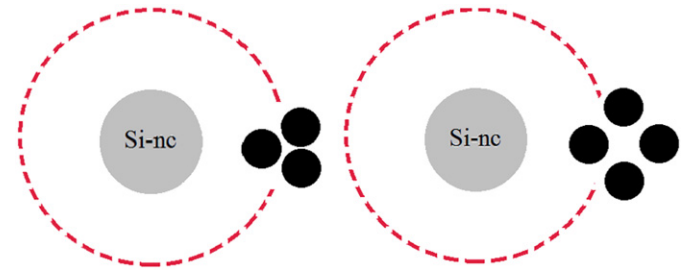


Fig. 8. Schematic illustration of ion triplet and ion quadruplet model.

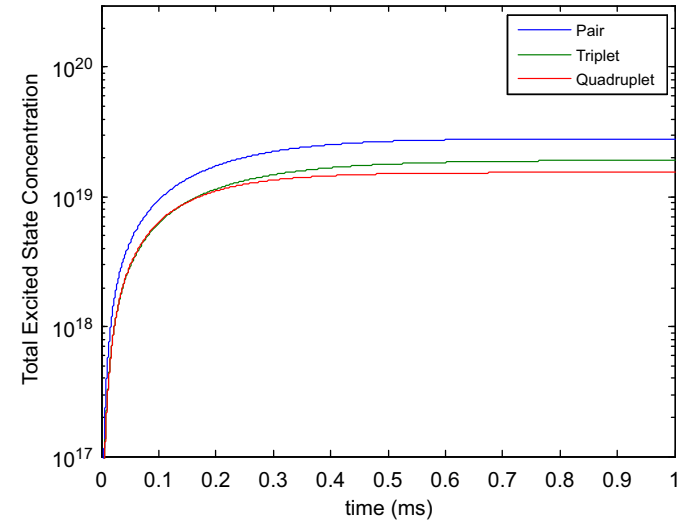


Fig. 9. Simulations of the rise dynamics for the ion pair, triplet, and quadruplet models.

5. Results and discussion

5.1. Simulations of indirect excitation: cluster size dependence

Fig. 9 shows simulations of the indirect excitation rise dynamics for the ion pair, ion triplet, and ion quadruplet models. We see that as cluster size increases, the total excited state fraction decreases. This is due to an increase in the amount of ion-ion interactions for increasing cluster sizes. The total excited

population among samples S1–S3 does not fully concur with results seen in Fig. 1. This result shows that the largest erbium signal comes from S3 (which has the smallest erbium clusters), which agrees with simulations in Fig. 9. However, from these simulations, we also expect that the smallest erbium signal should come from S2 (which has the largest erbium clusters), which we do not see in Fig. 1.

Fig. 10 shows simulations of the normalised decay transients for the ion pair, ion triplet, and ion quadruplet rate equation models. Table 3 summarises the fits for these transients. We see that as cluster size increases, the amplitude of the microsecond decay component becomes stronger, whereas the rate becomes slower.

We see in Fig. 10 that this simulation contradicts with what we observe experimentally; as erbium cluster size increases, the amplitude of the microsecond decay component becomes smaller

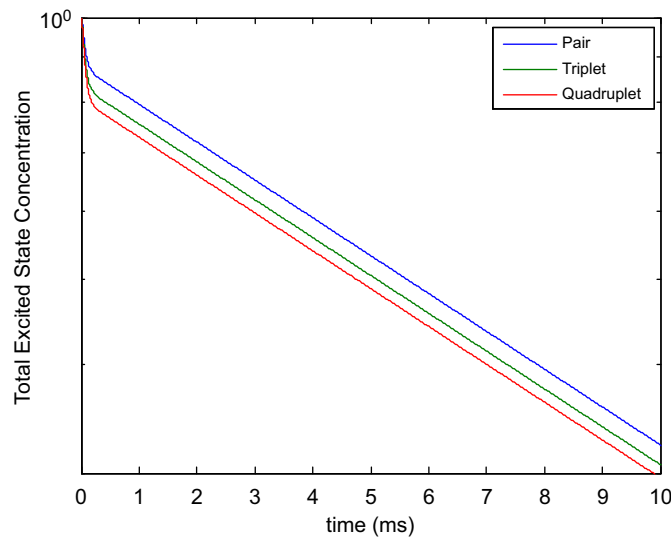


Fig. 10. Simulated decay transients for the ion pair, ion triplet, and ion quadruplet models.

Table 3
Fitting summary for simulated decay transients.

	t1 (us)	t2 (ms)	A	B
Pair	64.93	10	0.14	0.88
Triplet	65.07	10	0.19	0.83
Quadruplet	66.36	10	0.22	0.81

and its rate becomes faster. This, along with the observations of the total excited fraction, suggests that cluster size alone cannot explain the experimental observations.

5.2. Indirect excitation: Si-nc concentration, clustered fraction, and coupled proportion dependence

Other factors, along with cluster size, may also affect the decay dynamics. For example, we know that the amount of Si excess varies amongst samples S1–S3. Fig. 11 shows simulations of the amplitude and lifetime of the microsecond component as a function of Si-nc concentration, for the ion pair model. We see that as Si-nc concentration increases, the amplitude and lifetime of the microsecond component increases. We know that S3 has the most Si excess, and, therefore, this observation is in part agreement with experimental results. The same dependence of Si-nc concentration on the amplitude and lifetime of the microsecond component is obtained for the ion-triplet and ion-quadruplet geometries. However, the differences in Si excess between samples S1 and S3 are likely to be very small, and the simulation results show that the lifetimes are not very sensitive to changes in the Si-nc concentration.

It should be noted here that the previous models strictly assume that 100% of the erbium is clustered. In fact, this may not be the case. If the Er luminescence is entirely from Er₂O₃ clusters, then we would expect the PL spectra in Fig. 1 to show narrowing of the inhomogeneous broadening, which is not the case. The fraction of erbium ions that are clustered may have an effect on the decay dynamics. In order to assess this effect, a separate rate equation model that includes isolated ions as well as ion pairs was developed (see Appendix C). Fig. 12 shows the

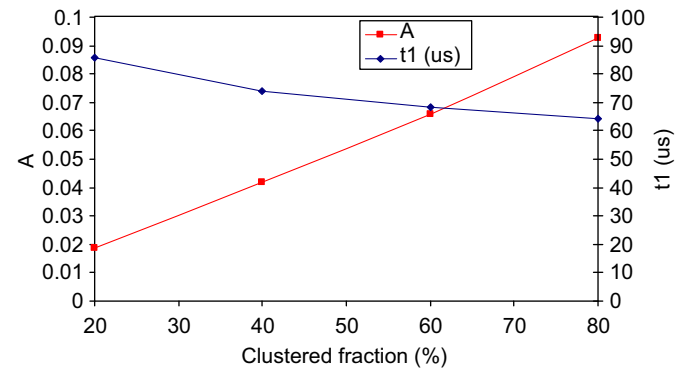


Fig. 12. Simulations of the amplitude and lifetime of the fast decay component as a function of the ion pair/isolated ion ratio.

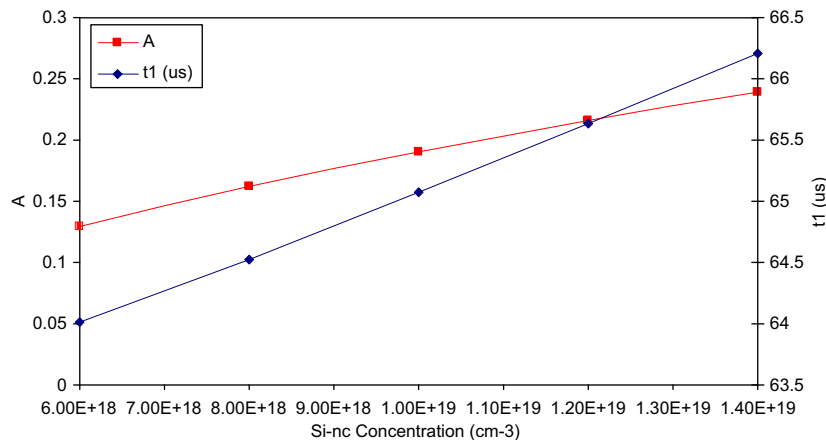


Fig. 11. Simulations of the amplitude and lifetime of the fast decay component as a function of Si-nc concentration.

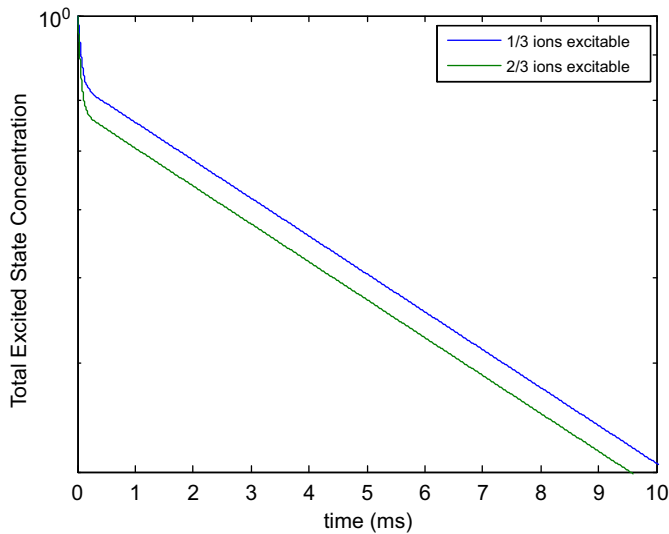


Fig. 13. Simulated decay transients of ion triplets with 1/3 ions coupled to Si-nc and 2/3 ions coupled to Si-nc.

Table 4
Fitting summary for simulated decay dynamics of cluster triplet models with 1/3 ions excitable and 2/3 ions excitable.

	t1 (us)	t2 (ms)	A	B
1/3	65.07	10	0.19	0.83
2/3	57.16	10	0.25	0.78

dependence of the amplitude and lifetime of the microsecond component as the ratio of the ion pairs/isolated ions increases. For a highly clustered erbium concentration, the microsecond component becomes stronger and faster.

The debate over the number of ions that can be excited through a single Si-nc has still yet to be resolved. Values ranging from 1 [15] up to 35 [13] have been reported. If the number is more than 1, then the assumption that only one ion within a cluster is coupled to the Si-nc may be invalid. Another rate equation model that treats the cluster as an ion-triplet has been developed, but with *two* out of three erbium ions coupled to the Si-nc. The effects of the proportion of the cluster that is coupled to the Si-nc on the decay dynamics were assessed using this model (see Appendix D). Fig. 13 shows the normalised simulated decay lifetimes for both cluster triplet geometries (1/3 ions coupled and 2/3 ions coupled). Table 4 summarises the double exponential fits for these two decay curves. We see that for the triplet model with 2/3 ions coupled, the amplitude becomes stronger and the lifetime becomes faster. This, in part, explains the small microsecond component amplitude observed for sample S2. This sample has the largest clusters (≈ 17 nm), and therefore it is reasonable to assume that the majority of the clusters remain outside of the Si-nc interaction region. For the smaller clusters evidenced in S1 and S3, a higher proportion of the clusters are expected to lie within the interaction region of the Si-nc, resulting in large microsecond component amplitudes.

5.3. Direct excitation: the dependence on the pumping rate

One may assume that, if the ion-ion interactions within clusters are responsible for the microsecond decay under indirect excitation, they should also be apparent under direct excitation. As seen in Fig. 2, under direct excitation, no microsecond decay component is observable. Fig. 14 shows simulated

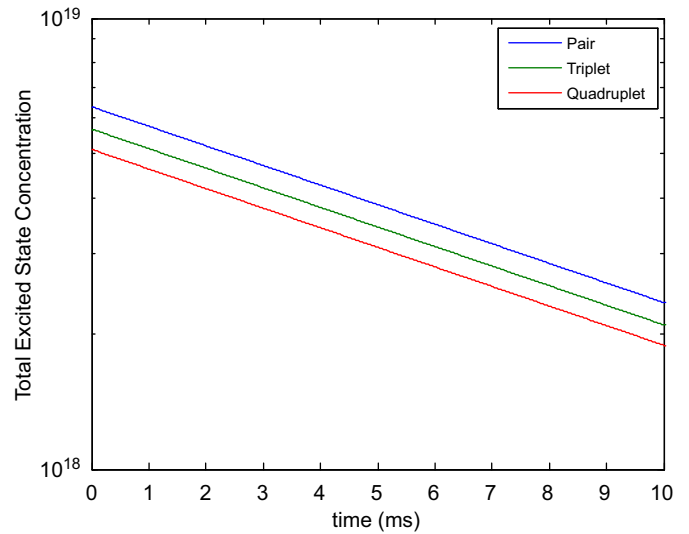


Fig. 14. Simulated decay data under direct excitation, for ion pair, triplet, and quadruplet models.

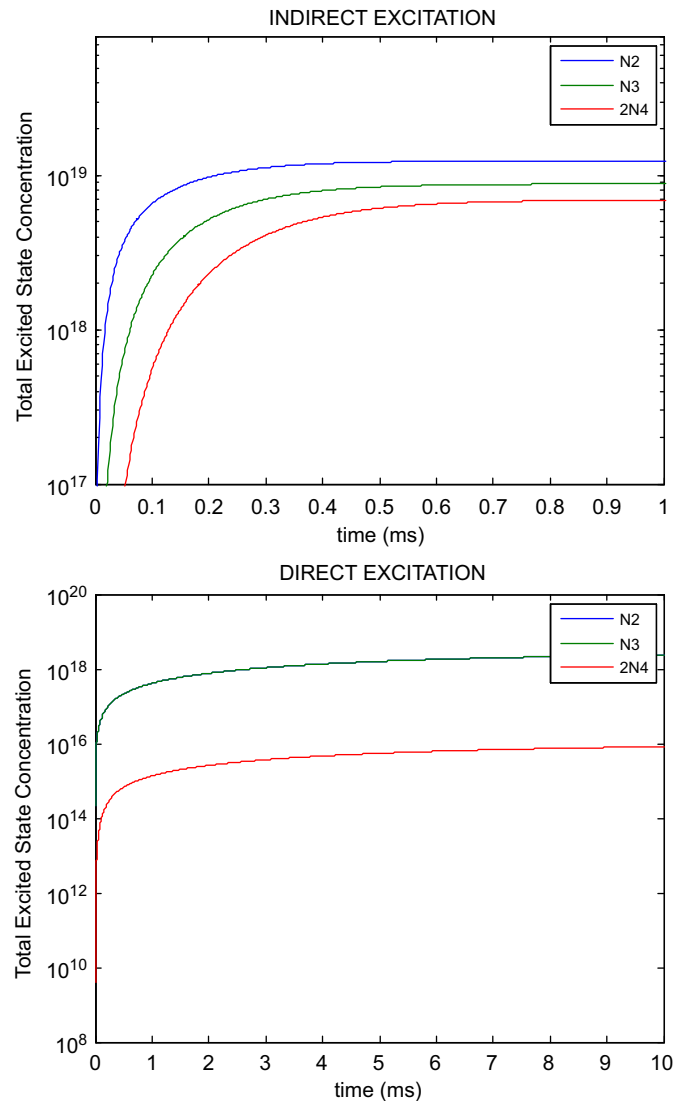


Fig. 15. Decomposed simulated rise data of the ion pair model, for both indirect (top) and indirect (bottom) excitation.

decay transients under direct excitation for the ion pair, triplet, and quadruplet models. Under direct excitation, no microsecond component is observable. The reason behind this will be explained through the ion pair model. In order for the microsecond component to become observable, the saturation level of the N_4 state (doubly excited pair) must be appreciably populated. This requires a pumping rate that is of the same order as the overall decay rate of each individual erbium ion. Under in-direct excitation, this requirement is satisfied; the pumping rate is given by the product of the Si-nc:erbium coupling co-efficient and the exciton concentration (A and n_b , respectively). For $A=3e-15 \text{ cm}^3 \text{ s}^{-1}$ and $n_b \approx 5e18 \text{ cm}^{-3}$, this gives a pumping rate of $\approx 15000 \text{ s}^{-1}$. However, for direct excitation, the pumping rate drops by 3–4 orders of magnitude. The pumping rate here is given by the product of the direct excitation cross section and the photon flux (B and φ_2 , respectively). For $B=1e-19$ and $\varphi_2=1.75e20$, this yields a pumping rate of 17.5, much lower than the rates required for the microsecond decay component to become observable. Fig. 15 shows the rise dynamics of the ion pair model under both direct and indirect excitation. The data is decomposed to show the contributions of the singly excited pairs (N_2, N_3) and the doubly excited pair (N_4). It is clear to see the differences in the saturated levels of N_4 under in-direct and direct excitation. It should also be noted that we may be exciting a much larger, and perhaps entirely different, population of erbium ions under direct excitation, giving reason for the slightly longer lifetimes observed in Table 1.

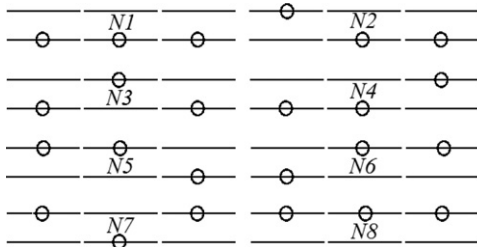
6. Conclusions

We have reported sensitization of erbium ions through Si-ncs evidenced by erbium emission from erbium doped Si-rich SiO_2 containing erbium clusters. As well as a relatively long lifetime component (10 ms), we also observe a microsecond decay component, attributable to the ion–ion interactions in erbium clusters. The clusters will play a key role in the in-direct sensitization process; only one ion in the cluster needs to be excited, and rapid energy migration will sensitise other ions in the cluster. The random nature of the microsecond decay component can be explained through changes in cluster size, the degree of Si-nc to erbium cluster coupling, and total clustered erbium fraction. These erbium ion–ion interactions could also explain the origins of the stretched and multi-exponential lifetimes in published literature.

Acknowledgements

The authors are grateful for the funding provided for this work by the Engineering and Physical Sciences Research Council.

Appendix A. Triplet rate states (top) and triplet equations (bottom)



$$\frac{dn_a}{dt} = -\sigma_{ab}\varphi_1 n_a + w_b n_b + An_b(N_1 + N_3 + N_4 + N_6)$$

$$\frac{dn_b}{dt} = \sigma_{ab}\varphi_1 n_a - w_b n_b - An_b(N_1 + N_3 + N_4 + N_6)$$

$$\frac{dN_1}{dt} = -An_b N_1 + w_{rad}(N_2 + N_3 + N_4) - 3BN_1\varphi_2$$

$$\frac{dN_2}{dt} = An_b N_1 + w_{Er}(N_3 + N_4 - 2N_2) + w_{rad}(N_5 + N_7 - N_2) + w_p(N_5 + N_7) + B\varphi_2(N_1 - 2N_2)$$

$$\frac{dN_3}{dt} = -An_b N_3 + w_{Er}(N_2 + N_4 - 2N_3) + w_{rad}(N_5 + N_6 - N_3) + w_p(N_5 + N_6) + B\varphi_2(N_1 - 2N_3)$$

$$\frac{dN_4}{dt} = -An_b N_4 + w_{Er}(N_2 + N_3 - 2N_4) + w_{rad}(N_6 + N_7 - N_4) + w_p(N_6 + N_7) + B\varphi_2(N_1 - 2N_4)$$

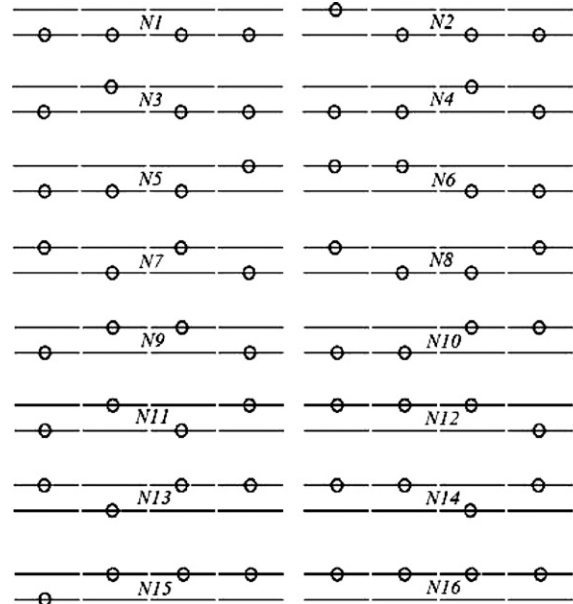
$$\frac{dN_5}{dt} = -An_b N_5 + w_{Er}(N_6 + N_7 - 2N_5) + w_{rad}(N_8 - 2N_5) + 2w_p(N_8 - N_5) + B\varphi_2(N_2 + N_3 - N_5)$$

$$\frac{dN_6}{dt} = -An_b N_6 + w_{Er}(N_5 + N_7 - 2N_6) + w_{rad}(N_8 - 2N_6) + 2w_p(N_8 - N_6) + B\varphi_2(N_3 + N_4 - N_6)$$

$$\frac{dN_7}{dt} = An_b N_4 + w_{Er}(N_5 + N_6 - 2N_7) + w_{rad}(N_8 - 2N_7) + 2w_p(N_8 - N_7) + B\varphi_2(N_2 + N_4 - N_7)$$

$$\frac{dN_8}{dt} = An_b N_6 - 3w_{rad}N_8 - 6w_pN_8 + B\varphi_2(N_5 + N_6 + N_7)$$

Appendix B. Quadruplet states (top) and rate equations (bottom)



$$\frac{dn_a}{dt} = -\sigma_{ab}\varphi_1 n_a + w_b n_b + An_b(N_1 + N_3 + N_4 + N_5 + N_9 + N_{10} + N_{11} + N_{15})$$

$$\frac{dn_b}{dt} = \sigma_{ab}\varphi_1 n_a - w_b n_b - An_b(N_1 + N_3 + N_4 + N_5 + N_9 + N_{10} + N_{11} + N_{15})$$

$$\frac{dN_1}{dt} = -An_bN_1 + w_{rad}(N_2 + N_3 + N_4 + N_5) - 4BN_1\varphi_2$$

$$\frac{dN_2}{dt} = An_bN_1 + w_{Er}(N_3 + N_4 + N_5 - 3N_2) + w_{rad}(N_6 + N_7 + N_8 - N_2) + w_p(N_6 + N_7 + N_8) + B\varphi_2(N_1 - 3N_2)$$

$$\frac{dN_3}{dt} = -An_bN_3 + w_{Er}(N_2 + N_4 + N_5 - 3N_3) + w_{rad}(N_6 + N_9 + N_{11} - N_3) + w_p(N_6 + N_9 + N_{11}) + B\varphi_2(N_1 - 3N_3)$$

$$\frac{dN_4}{dt} = -An_bN_4 + w_{Er}(N_2 + N_3 + N_5 - 3N_4) + w_{rad}(N_7 + N_9 + N_{10} - N_4) + w_p(N_7 + N_9 + N_{10}) + B\varphi_2(N_1 - 3N_4)$$

$$\frac{dN_5}{dt} = -An_bN_5 + w_{Er}(N_2 + N_3 + N_4 - 3N_5) + w_{rad}(N_8 + N_{10} + N_{11} - N_5) + w_p(N_8 + N_{10} + N_{11}) + B\varphi_2(N_1 - 3N_5)$$

$$\frac{dN_6}{dt} = An_bN_3 + w_{Er}(N_7 + N_8 + N_9 + N_{11} - 4N_6) + w_{rad}(N_{12} + N_{14} - 2N_6) + 2w_p(N_{12} + N_{14} - N_6) + B\varphi_2(N_2 + N_3 - 2N_6)$$

$$\frac{dN_7}{dt} = An_bN_4 + w_{Er}(N_6 + N_8 + N_9 + N_{10} - 4N_7) + w_{rad}(N_{12} + N_{13} - 2N_7) + 2w_p(N_{12} + N_{13} - N_7) + B\varphi_2(N_2 + N_4 - 2N_7)$$

$$\frac{dN_8}{dt} = An_bN_5 + w_{Er}(N_6 + N_7 + N_{10} + N_{11} - 4N_8) + w_{rad}(N_{13} + N_{14} - 2N_8) + 2w_p(N_{13} + N_{14} - N_8) + B\varphi_2(N_2 + N_5 - 2N_8)$$

$$\frac{dN_9}{dt} = -An_bN_9 + w_{Er}(N_6 + N_7 + N_{10} + N_{11} - 4N_9) + w_{rad}(N_{12} + N_{15} - 2N_9) + 2w_p(N_{12} + N_{15} - N_9) + B\varphi_2(N_3 + N_4 - 2N_9)$$

$$\frac{dN_{10}}{dt} = -An_bN_{10} + w_{Er}(N_7 + N_8 + N_9 + N_{11} - 4N_{10}) + w_{rad}(N_{13} + N_{15} - 2N_{10}) + 2w_p(N_{13} + N_{15} - N_{10}) + B\varphi_2(N_4 + N_5 - 2N_{10})$$

$$\frac{dN_{11}}{dt} = -An_bN_{11} + w_{Er}(N_6 + N_8 + N_9 + N_{10} - 4N_{11}) + w_{rad}(N_{14} + N_{15} - 2N_{11}) + 2w_p(N_{14} + N_{15} - N_{11}) + B\varphi_2(N_3 + N_5 - 2N_{11})$$

$$\frac{dN_{12}}{dt} = An_bN_9 + w_{Er}(N_{13} + N_{14} + N_{15} - 3N_{12}) + w_{rad}(N_{16} - 3N_{12}) + w_p(3N_{16} - 6N_{12}) + B\varphi_2(N_6 + N_7 + N_9 - N_{12})$$

$$\frac{dN_{13}}{dt} = An_bN_{10} + w_{Er}(N_{12} + N_{14} + N_{15} - 3N_{13}) + w_{rad}(N_{16} - 3N_{13}) + w_p(3N_{16} - 6N_{13}) + B\varphi_2(N_7 + N_8 + N_{10} - N_{13})$$

$$\frac{dN_{14}}{dt} = An_bN_{11} + w_{Er}(N_{12} + N_{13} + N_{15} - 3N_{14}) + w_{rad}(N_{16} - 3N_{14}) + w_p(3N_{16} - 6N_{14}) + B\varphi_2(N_6 + N_8 + N_{11} - N_{14})$$

$$\frac{dN_{15}}{dt} = -An_bN_{15} + w_{Er}(N_{12} + N_{13} + N_{14} - 3N_{15}) + w_{rad}(N_{16} - 3N_{15}) + w_p(3N_{16} - 6N_{15}) + B\varphi_2(N_9 + N_{10} + N_{11} - N_{15})$$

$$\frac{dN_{16}}{dt} = An_bN_{15} - 4w_{rad}N_{16} - 12w_pN_{16} + B\varphi_2(N_{12} + N_{13} + N_{14} + N_{15})$$

Appendix C. Isolated and paired rate equation model

$$\frac{dn_a}{dt} = -\sigma_{ab}\varphi_1n_a + w_bn_b + An_b(N_1 + N_3 + N_4)$$

$$\frac{dn_b}{dt} = \sigma_{ab}\varphi_1n_a - w_bn_b - An_b(N_1 + N_3 + N_4)$$

$$\frac{dN_1}{dt} = -An_bN_1 + w_{rad}N_2 - BN_1\varphi_2$$

$$\frac{dN_2}{dt} = An_bN_1 - w_{rad}N_2 + BN_1\varphi_2$$

$$\frac{dN_3}{dt} = -An_bN_3 + w_{rad}(N_4 + N_5) - 2BN_3\varphi_2$$

$$\frac{dN_4}{dt} = An_bN_3 + w_{Er}(N_5 - N_4) + w_{rad}(N_6 - N_4) + w_pN_6 + B\varphi_2(N_3 - N_4)$$

$$\frac{dN_5}{dt} = -An_bN_5 + w_{Er}(N_4 - N_5) + w_{rad}(N_6 - N_5) + w_pN_6 + B\varphi_2(N_3 - N_5)$$

$$\frac{dN_6}{dt} = An_bN_5 - 2w_{rad}N_6 - 2w_pN_6 + B\varphi_2(N_4 + N_5)$$

Appendix D. 2nd triplet rate equation model

$$\frac{dn_a}{dt} = -\sigma_{ab}\varphi_1n_a + w_bn_b + An_b(2N_1 + N_2 + N_3 + 2N_4 + N_6 + N_7)$$

$$\frac{dn_b}{dt} = \sigma_{ab}\varphi_1n_a - w_bn_b - An_b(2N_1 + N_2 + N_3 + 2N_4 + N_6 + N_7)$$

$$\frac{dN_1}{dt} = -2An_bN_1 + w_{rad}(N_2 + N_3 + N_4) - 3BN_1\varphi_2$$

$$\frac{dN_2}{dt} = An_b(N_1 - N_2) + w_{Er}(N_3 + N_4 - 2N_2) + w_{rad}(N_5 + N_7 - N_2) + w_p(N_5 + N_7) + B\varphi_2(N_1 - 2N_2)$$

$$\frac{dN_3}{dt} = An_b(N_1 - N_3) + w_{Er}(N_2 + N_4 - 2N_3) + w_{rad}(N_5 + N_6 - N_3) + w_p(N_5 + N_6) + B\varphi_2(N_1 - 2N_3)$$

$$\frac{dN_4}{dt} = -2An_bN_4 + w_{Er}(N_2 + N_3 - 2N_4) + w_{rad}(N_6 + N_7 - N_4) + w_p(N_6 + N_7) + B\varphi_2(N_1 - 2N_4)$$

$$\frac{dN_5}{dt} = An_b(N_2 + N_3) + w_{Er}(N_6 + N_7 - 2N_5) + w_{rad}(N_8 - 2N_5) + 2w_p(N_8 - N_5) + B\varphi_2(N_2 + N_3 - N_5)$$

$$\frac{dN_6}{dt} = An_b(N_4 - N_6) + w_{Er}(N_5 + N_7 - 2N_6) + w_{rad}(N_8 - 2N_6) + 2w_p(N_8 - N_6) + B\varphi_2(N_3 + N_4 - N_6)$$

$$\frac{dN_7}{dt} = An_b(N_4 - N_7) + w_{Er}(N_5 + N_6 - 2N_7) + w_{rad}(N_8 - 2N_7) + 2w_p(N_8 - N_7) + B\varphi_2(N_2 + N_4 - N_7)$$

$$\frac{dN_8}{dt} = An_b(N_6 + N_7) - 3w_{rad}N_8 - 6w_pN_8 + B\varphi_2(N_5 + N_6 + N_7)$$

References

- [1] A.J. Kenyon, P.F. Trwoga, M. Federighi, C.W. Pitt, *J. Phys. Condens. Matter* 6 (1994) L319.
- [2] M. Fujii, M. Yoshida, S. Hayashi, K. Yamamoto, *J. Appl. Phys.* 84 (1998) 4525.
- [3] A.J. Kenyon, et al., *J. Appl. Phys.* 91 (2002) 367.
- [4] B. Garrido, C. García, P. Pellegrino, D. Navarro-Urrios, N. Dalosso, L. Pavesi, F. Gourbilleau, R. Rizk, *Appl. Phys. Lett.* 89 (2006) 163103.
- [5] E. Delevaque, T. Georges, M. Monerie, P. Lamouler, J.-F. Bayon, *Photonics Technol. Lett.* 5 (1993) 73.
- [6] I.Y. Kim, J.H. Shin, K.J. Kim, *Appl. Phys. Lett.* 95 (2009) 221101.
- [7] I. Izuddin, A. Moskalenko, I. Yassievich, M. Fujii, T. Gregorkiewicz, *Phys. Rev. Lett.* 97 (2006) 207401.
- [8] A. Al Choueiry, A.M. Jurdyc, B. Jacquier, F. Gourbilleau, R. Rizk, *J. Appl. Phys.* 106 (2009) 053107.
- [9] D. Navarro-Urrios, A. Pitanti, N. Dalosso, F. Gourbilleau, R. Rizk, B. Garrido, L. Pavesi, *Phys. Rev. B* 79 (2009) 193312.
- [10] X. Wang, P. Li, M. Malac, R. Lockwood, A. Meldrum, *Phys. Status Solidi (c)* 8 (2011) 1038.
- [11] D.A. Stanley, H. Alizadeh, A. Helmy, N.P. Kherani, L. Qian, S. Zukotynski, *J. Lumin.* 131 (2011) 72.
- [12] M. Digonnet, *Opt. Fiber Technol.* 1 (1994) 48.
- [13] D. Pacifici, G. Franzò, F. Priolo, F. Iacona, L. Dal Negro, *Phys. Rev. B* 67 (2003) 1.
- [14] B. Garrido, C. García, S.-Y. Seo, P. Pellegrino, D. Navarro-Urrios, N. Dalosso, L. Pavesi, F. Gourbilleau, R. Rizk, *Phys. Rev. B* 76 (Dec. 2007) 1.
- [15] P.G. Kik, M.L. Brongersma, A. Polman, *Appl. Phys. Lett.* 76 (2000) 2325.